Original Research Article

In-silico Design of Oxadiazole Hybrids as Potential Inhibitors of Dengue Virus NS2B-NS3 Protease

Samuel Ndaghiya Adawara[1],* , Gideon Shallangwa Adamu[2] , Paul Andrew Mamza[2], Ibrahim Abdulkadir[2]

[1] Department of Pure and Applied Chemistry, Faculty of Science, University of Maiduguri, P.M.B. 1069, Maiduguri, Borno State, Nigeria

[2] Department of Chemistry, Faculty of Physical Sciences, Ahmadu Bello University, P.M.B. 1044, Zaria, Kaduna State, Nigeria

ARTICLE INFO

ABSTRACT

This study aimed at designing highly potent dengue virus (DENV) inhibitors targeting the NS2B-NS3 protease from 1,2-benzisothiazol-3(2H)-one-1,3,4-oxadiazole (BTZO) hybrid through quantitative-structure-activity relationship (QSAR) and subsequently structure-based design, molecular docking, and ADMET (Adsorption-Distribution-Metabolism-Excretion Toxicity) of the designed BTZO derivatives. A QSAR model was developed to correlate the biological activity with the descriptor calculated from the BTZO hybrid using multiple linear regression. The model was validated and the information from the model was used to design more potent derivatives which were evaluated through molecular docking and ADMET prediction. The QSAR model showed good statistical quality ($R^2_{Training}$ = 0.89228, $R^2_{predicted}$ = 0.72734 $R^2_{adjusted}$ = 0.87074, Q^2_{LOO} = 0.81896, and cR^2p = 0.8154) leading to the design of nine active BTZO derivatives with better inhibitory activity than the lead compound (7n). A binding score of -23.731, -20.210, -23.568 kcal/mol better than Panduratin and Ribavirin (-14.1715, -17.2571 kcal/mol) for compounds C-148, C-205, and C-206 respectively were obtained, including good ADMET properties. This discovery not only aided in understanding the binding manner of BTZO hybrid to the NS2B-N3 targets but also provided information for the development of active NS2B-N3 protease inhibitors.

GRAPHICAL ABSTRACT
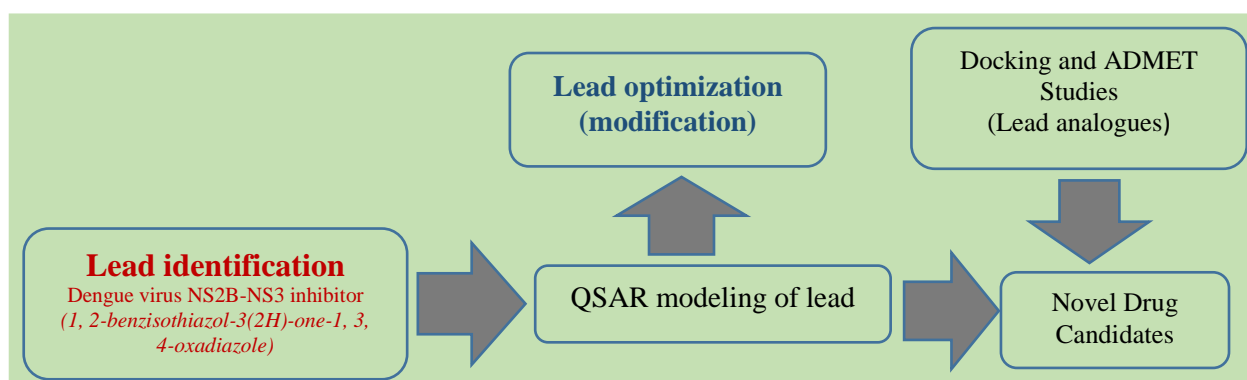
Introduction

Dengue virus is an important class of virus of the Flavivirus family that is accountable for the major cause of dengue fever, which could progress to dengue shock syndrome (DSS) which is all life-threatening symptoms of the dengue infection. Hence, constitute a major threat to the global community due to recurrent outbreaks in several parts of the world, which is facilitated by urbanization as well as world travel. Several attempts have been made by researchers to curb the menace of its infection in the forms of vaccination and drug treatment [1-2]. The roles of NS2B-NS3 and NS5 of among the seven non-structural proteins encoded by Flaviviruses are known, which include involvement in the replication of the virus [3-4], hence representing a viable target for the development of an anti-viral drug against the Flavivirus of interest.

In recent times, the DENV NS2B-NS3 non-structural viral proteases have become an increasingly important target for anti-dengue therapeutics development [5]. The number of people suffering from an infection instigated by the DENV has been estimated to be over 100 million every year and over 2.5 billion persons are likely to be infected globally. The outbreak of dengue virus infection has been reported in the various geographical region of the world at an epidemic level followed by a recurrent outbreak in some regions [6].

Despite the life-threatening perils, such as the risk of a DSS and dengue hemorrhagic fever in untreated individuals resulting from an infection related to the dengue virus, there are presently no appropriate antiviral agents against dengue viral related infection [7].

Chemometric approaches involving molecular modelings such as molecular docking, QSAR, and drug database search have led to the identification of some potential Flavivirus NS2B-NS3 inhibitors towards drug development [8]. The utilization of *in silico* method in the development and identification of novel NS2B-NS3 inhibitors has been reported [8-12]. QSAR chemometric approach which relates the biological activities of chemical compounds such as IC_{50}, CC_{50} to their structural information has been regarded as the main instrument in the modern drug design process and screening of potentially active compounds from drug libraries or collection of compounds [13-14]. Also, *in silico* approaches have the advantage of complementing existing in vitro biological activity methodologies, allowing for faster drug development while avoiding the time, cost, and inconvenience of animal testing. Multiple linear regression has been employed to create a quantitative relationship between molecular structural information (descriptors) some potential active compounds with their biological activities, subsequently *in silico* screening is adopted to the QSAR model to predict the structure of the new potentially active compounds [14].

This study aimed to explore ligand-based drug approaches to propose new BTZO hybrid derivatives as dengue virus inhibitors. Herein this theoretical investigation, computational approaches of QSAR molecular docking and ADME prediction were used to explore the basic molecular information responsible for the biological activity of the compounds and the interaction of DENV NS2B-NS3 inhibitory agents for the target pockets of the receptor.

Derivatives of 1, 2-benzisothiazol-3(2H)-one serve an important role in a variety of medicinal applications. 1,2-benzisothiazol-3(2H)-ones are an important class of heterocyclic compounds with a wide range of therapeutic potential. Suitably modified 1, 2-benzisothiazol-3(2H)-ones have been demonstrated to have significant antiviral activity. Compounds with a 1, 3, 4-oxadiazole framework have also gotten a lot of attention in medicinal research, because this structural motif has been used in a wide range of applications [15].

The study will shed light on the essential structural features and chemical changes required for the BTZO derivatives to possess improved inhibitory biological activities against DENV NS2B-NS3, as well as pave way for a new view to explore the most potent and efficient drug design to overcome the dengue virus and treat its fatal consequences on human health. This study may well have a significant impact on drug design and development approaches by reducing experimental costs and stages.

Methods

Set of data

A series of twenty-four sets of BTZO hybrid analogues available in Supplementary Data Table 1 (Table SD1) retrieved from literature was used as the biological data set in this research [15]. The 2-D structures of the considered data (BTZO) were sketched with the aid of ChemDraw Ultra v.11.0 software [16] (Table SD1).

Their experimentally evaluated biological activity as dengue virus inhibitors was reported as percentage inhibition by the authors at 25 µM dose [15]. The percentage inhibition activity data (*%I*) for each compound was converted to a logarithmic unit to obtain linearity in the data for the QSAR study. The data transformation was accomplished using Equation 1 as described by other authors for such data [17-18].

$$\mathbf{pI} = log\left[\frac{\%I}{(100-\%I)}\right] \tag{1}$$

Data computation, pretreatment, and partition

The drawn 2-D structures of the BTZO derivatives were optimized for energy minimization by Spartan 14 software [19], to obtain them in their best conformation as well as calculation of some quantum chemical descriptor using 6-31G* basis set of B_3LYP theory level of density functional theory. Other descriptors were also generated from the minimized structure of

each of the compounds using Padel-Descriptor software [20]. The calculated descriptors were subjected to pretreatment [21] to remove redundant as well as intercorrelated data among them to avoid over-fitting.

To build a model, the compounds alongside their respective descriptors were subsequently grouped into training and test sets, the two sets were made in such a manner that the training set makes up about 70 percent of the data for the model building while the remaining 30 percent makes up the test set for model evaluation. The data division was achieved using the data division package (DatasetDivision 1.2) [21] which utilizes the Kennard-Stone algorithm [22] in the process.

Model generation selection and statistical justification

The model building was achieved with the use of the DTC lab tool (MLR BestSubsetSelection 1.2) [23] described in our previous work. The model development involves the use of the train set only to select the set of descriptors that are best related to the biological activity (pI). The individual descriptors that collectively describe a model are presented in Table SD2.

Statistical Internal and external model authentication

After the model generation using the descriptor, the top-ranked model was selected for further external validation. The model selection is based on some recommended criteria called internal validation [23-25]. The minimum recommended acceptable values (threshold) for QSAR model validation parameter and some of the obtained recommended criteria for internal and external validations of the developed model are presented in Table 1, such as correlation factor (R^2). To determine the reliability, stability, extrapolative power, and robustness of the model. The validation factors considered include all the

parameters presented in Tables 1 and SD3. The applicability domain was also established to check for the inter-correlation effect defined by a

variance inflation factor (VIF), another model statistical authentication factor such as the Y-scrambling test was also carried out.

Table 1. Developed model score and validation threshold factors for an acceptable QSAR model

Statistical Validation parameter	Recommended Threshold	Model Score (Equation 7)	Statement
Coefficient of determination (R^2)	≥ 0.6	0.89228	Excellent
Predicted Coefficient of determination (R^2_{pred})	> 0.5	0.72734	Highly predictive
Cross-validation coefficient (Q^2_{CV})	> 0.5	0.81896	Reliable
Difference between R^2 and Q^2_{CV} ($R^2 - Q^2_{CV}$)	≤ 0.3	0.07332	
Y-randomization coefficient (cR^2_p)	> 0.5	0.815428	Robust
Adjusted R-squared (R^2_{adj})	> 0.5	0.87074	Stable
Variance inflation factor (VIF)	< 10	1.05-1.14	True model

Variance inflation factor test

The existence of multi-collinearity between the independent variables (descriptors) within the model was evaluated through the use of Equation 2 called variance inflation factor (V.I.F),

$$(V.I.F)_i = \left(1 - R^2_{ij}\right)^{-1} \quad (2)$$

From Eq. 2, R^2_{ij} describes the factor of the regression between the independent variable i concerning other variables j within the same model [15].

Domain of applicability

The applicability domain (AD) of a model helps in the finding or avoiding the use of the dissimilar compound in the development of the model that could wrongly predict the activity of compounds that don't belong to the same class [26]. The leverage-based applicability domain approach which is the corresponding transverse component of the hat matrix (HATM); leverage (hi) and standardized residual (SDR) values plot was used to define to establish the AD (William's plot) [27, 26].

A compound is considered outside the domain if its leverage (hi) value exceeds a threshold value (h*) of $0 < h_i < h*$ and $-3 < SDR < 3$. Herein, each compound's h_i was evaluated from the

component of the transverse component of the HATM using Eq. 3.

$$HATM = H.(H^T H)^{-1}.H^T \quad (3)$$

From Eq. 3, H describes the descriptors matrix and H^T is its inverse, while the SDR was evaluated using Eq. 4.

$$SDR = \frac{\hat{r} - r}{\sqrt{\frac{\sum_{i=1}^{n}(\hat{r} - r)^2}{p}}} \quad (4)$$

The r and $\hat{r}$ from Eq. 4 are the experimental and predicted activity of the sets correspondingly, while p gives the number of molecules in the considered set.

The cautionary leverage for the applicability domain was obtained from Eq. 5.

$$h* = \frac{3.(j+1)}{p} \quad (5)$$

The j in Eq. 5 is the sum of independent variables (descriptors) existing in the model, whereas p is the sum of molecules used in developing the model training set.

Y- Scrambling assessment for the robustness of MLR model

This assessment involves the haphazard generation of models by shambling the dependent variable randomly while leaving the independent variables unchanged. After such

shambling low R^2 and Q^2 values obtained confirms the robustness of the built model, such evaluation is also defined by the coefficient of randomization (cRp^2), which should not be less than 0.5 for a model to be considered valid and robust [27].

$$cRp^2 = R.(R^2 - (Rr)^2)^{1/2} \qquad (6)$$

From Eq. 6, average Rr = average 'R' of random models.

In-silico design of the novel BTZO derivatives through the ligand-based process and activity prediction

The molecular structural information revealed by the developed models to be responsible for the predicted activity (pI) of the BTZO derivatives were used in designing other derivatives of the studied compounds towards obtaining a hypothetically more potent derivative. This process involves the selection of the lead compounds and subsequent structural modification guided by the descriptors in the models and their relative significance concerning one another in predicting the biological activity of the lead compound from the data set (7n) selected herein owing to its high percentage inhibition activity values within the series of the studied compounds. The activity (pI) of each designed compound was predicted using Eq. 7 as well as its leverage to ensure that it is not a structural outlier [28-29].

Molecular docking Analysis of the designed compounds

Ligand/target pre-docking preparation

Since the DENV NS2B/NS3 protease is our target in this work, its structure reported by Noble and co-researcher [30] with the Protein Data Bank (PDB) ID 3U1I was downloaded from the RCSB database in complex with other ligands.

The obtained co-crystallized crystal structure of the protease (PDB code: 3U1I) with other ligands

as well as water molecules was subjected to preparation before the docking process. The preparation of the protease (PDB code: 3U1I) protease was done using Discovery Studio Visualizer as described in our previous work [14] [31].

Docking calculation

We accomplished molecular docking calculation for the evaluation of the binding mode/affinity between the receptor and the ligand with the aid of the ICM-Molsoft (http://www.molsoft.com/servers.html) [32]. The protease preparation before the docking calculations as well as the binding interaction mode visualization was achieved using Discovery Studio 2017. The protease preparation process and the docking process between the compounds and the protease have been described in the literature [33].

Following the successful completion of the docking runs, alternative conformations of the complexes were retrieved as well as their respective docking scores (kcal/mol), and the stable one having the most negative binding score was chosen as the optimal pose [34]. The ligand-protease complexes interactions were observed using the Discovery Studio Visualizer software [31]

ADMET prediction

To avoid potential pitfalls of the potential drug candidates of interest, it is necessary to carry some assessment of the metabolism of such drug candidates. In this, the drug-likeness, as well as pharmacokinetic studies, are governed by some parameters that are defined by Lipinski's rule of five. The ADMET predictions of the designed BTZO analogues were accomplished through the use of SwissADME/pkCSM – pharmacokinetics (http://biosig.unimelb.edu.au/pkcsm/) [35-36].

Results

Model and statistical authentication

The QSAR model is represented by Eq. 7, while the validation factors thresholds of the model as well as some of its statistical validation scores are presented in Table1.

The plots of experimental and predicted activity of both train and test sets of the model are presented in Figures 1 and 2 respectively, whereas the AD plot presented in Figure 3.

The model's descriptors correlation matrix, definitions, mean effect and V.I.F are presented in Table 2.

Prediction and validation of the activity of designed compounds

The calculated descriptor of the designed BTZO derivative predicted activity as well as their leverages are presented in Table 3, while the 2-D structure structures of the most active derivatives (C148, C-203, C-205 and C-206) are shown in Figure 4.

Docking Simulation Studies of the designed compounds

Figure 5 represents the 3D docking mode of the co-crystalised native ligand of the DENV protease (PDB code: 3U1I) and the designed compound with the best docking score (C-148)

The results of the docking showing various interaction energy terms for the designed compounds are presented in Table 4. The 2D interaction with the active site amino acid of the receptor is shown in Figures 6a-6f.

Drug-likeness, pharmacokinetics, and ADMET profile of the designed BTZO derivatives

The drug-likeness, pharmacokinetics, and ADME as well as the toxicity profile of the designed BTZO derivatives are presented in Tables 5 and 6 respectively.

Discussion

QSAR Model analysis

Model and statistical authentication

To establish a relationship in form of a model between the dengue virus inhibitory biological activity (pI) of the BTZO derivatives (ligands). The train set of the derivatives earlier obtained was used in building QSAR based model using the multiple linear regression (MLR) statistical methods. The model is represented by Eq. 7, which contains three independent variables that are determinant activity (pI) of the compounds which are AMR, AATSC7c, and E3u.

$$\textbf{pI} = -7.96196(+/-0.96522) +0.01807(+/-0.0031) \textbf{AMR} -124.53996(+/-31.15666) \textbf{AATSC7c} +12.28109(+/-2.14162)\textbf{E3u} \qquad (7)$$

After establishing the relationship between the independent variable and the activity, the reliability, robustness, stability, and predictive influence of the model was established against some standard recommended statistical validation factors that characterized the robust QSAR model. The recommended external and internal statistical validation factors are presented in Tables 1, and SD3.

The generated using descriptors obtained from a set of 19 BTZO derivatives and validated externally using 5 compounds as well as prediction of their activity (pI). The validation parameters obtained for the evaluation of the model validity include a correlation value of 0.89228, a cross-validated value of 0.81896, an adjusted correlation value of 0.87074, and a predicted correlation value of 0.72734. Other parameters suggested by Roy et al., for further evaluation of model quality are presented in Table SD3 [25]. Our model could be considered a robust one because all the correlation values considered are much greater than the 0.5 threshold limit and Golbraikh and Tropsha factors [24] are obeyed which suggests a robust and valid QSAR model as presented in Tables 1 and SD3, these results were further confirmed by

the lower difference between Q^2 and R^2 value of less than 0.03.

The validation of the model was further supported by the close agreement between the experimental and predicted activity (pI) for both train and test sets (Figures 1 and 2) with correlation values of greater than 0.5, with significantly low differences between them. Table SD2 showed a close agreement between them, this attests to the consistency of the model.
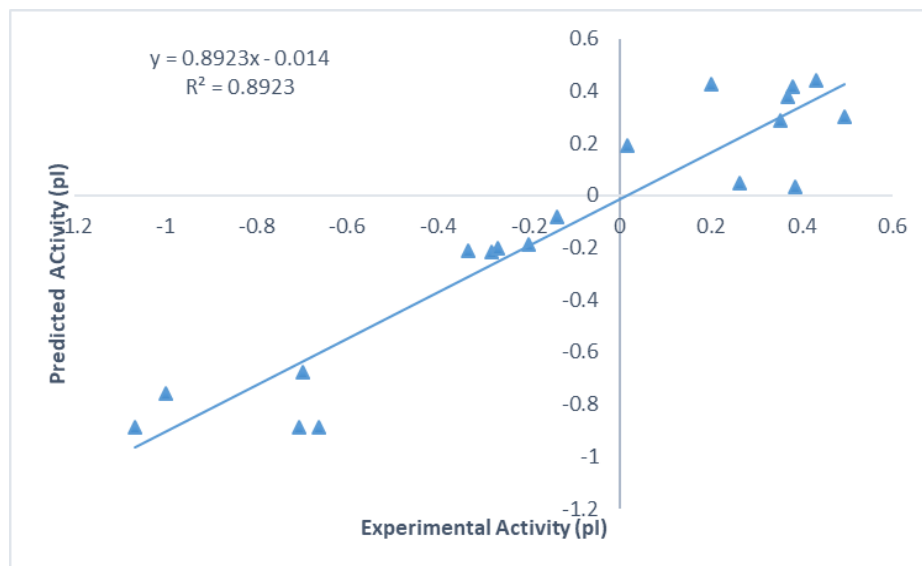
Figure 1. The experimental against predicted activities plot for the train set
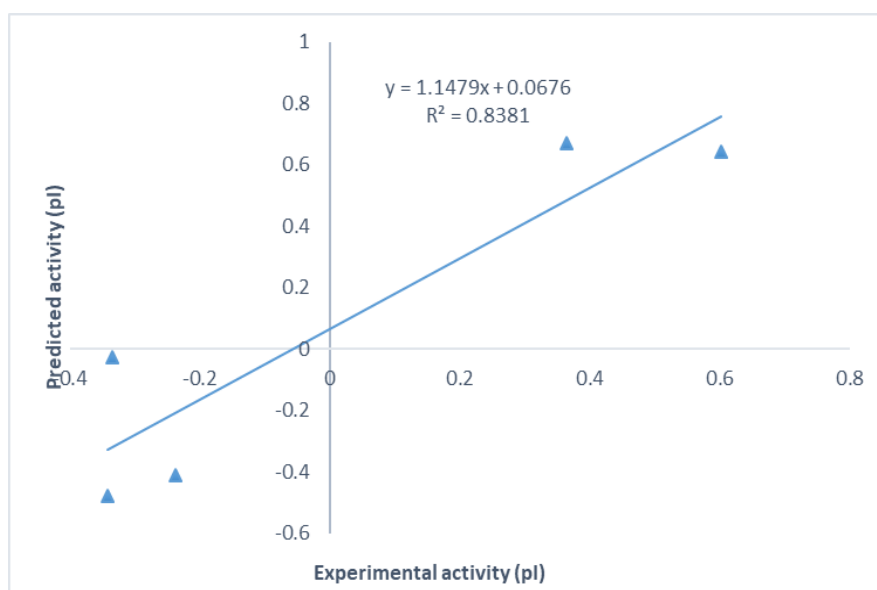
Figure 2. The experimental against predicted activities plot of the test set

A QSAR model obtained by chance could make an unreliable prediction due to multi-collinearity within the descriptors contained in a model; the presence of such a problem could be overcome through the evaluation of V.I.F. The obtained V.I.F values of all the independent variables (descriptors) in Equation 7, presented in Table 2 are all within the suggested acceptable value of less than 10 for confirmation of error associated with multi-collinearity that characterized a

coincidentally obtained model. Hence, our developed model was not obtained by chance but systematically established [14]. The correlation matrix of the descriptors also confirmed the absence of multi-collinearity within the descriptors as there is no dependency among them.

The Y-scrambling test for ten random runs characterized by a high coefficient of the randomization cRp^2 value of more than 0.5 and low Q^2 and R^2 values (Table SD4) was obtained for this test hence demonstrates reliability which entails a true QSAR model and that the built model is not accidental. Other significant statistical factors have been identified, and the Golbraikh and Tropsha conditions [24] have been highlighted to emphasize their significance in the

QSAR model validation (Table 2). The numerical values of selected independent variables in the model have been provided in Table SD3.

Outlier detection

The plot of the AD analysis using William's plot is represented in Figure 3. The plot (Figure 3) indicated that the compounds are all inside the AD (h*= 0.63 (Eq.5), SDR limit of ±3 (Eq.4)). The nonappearance of any of the compounds outside the limit boundaries (Figure 3) confirms the absence of outlier in the predictions by the model, [37] thus, the AD of the model is reasonable. For any compound to fit into the AD of the model, it has to be analogous to the ones from which the model is developed [38].
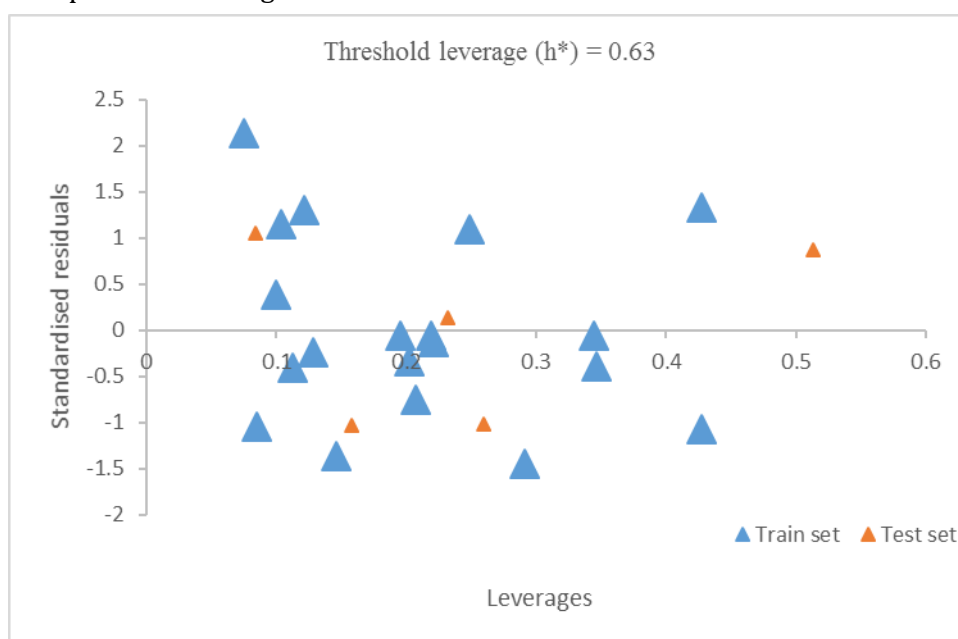
Figure 3. Graphical representation of the AD (Vertical and horizontal lines both indicating limit boundary (threshold))

Descriptors description and significance

The model's (Eq. 7) descriptors (independent variable) meaning, mean effect which quantifies the contributory level of each descriptor towards the dependent variable are presented in Table 2. AMR is the Molar refractivity, while E3u is the 3rd component accessibility directional WHIM

index/un-weighted AATSC7c is the spatial distribution function that describes the degree of the correlation between variables (molecular property) and the distance between them (lag) [39-40] which is evaluated by considering a set of atoms as discrete position in space while atomic property as the obtained position. The

mean effect of the descriptor AMR, AATSC7c and E3u were obtained in the order of E3u > AMR > AATSC7c (0.737073 > 0.271791> -0.00886).

The E3u had the maximum influence followed by AMR and lastly the AATSC7c. The positive mean effect values of AMR and E3u entail an improvement in the activity with an increase in their value, while the negative contribution of the AATSC7c descriptor means that atomic charge had a decreasing effect on the activity of the compound and that decrease in the value of such parameter could lead to better activity.

The obtained statistical P-value of less than 0.05 which relates to model quality on two variances at 95% confidence level presented in Table 2 entails a good quality model [41].

Table 2. Descriptor's correlation matrix, variance inflation, factor mean effect and P-value

Descriptor	AMR	AATSC7c	E3u	ME	VIF	P- value
AMR: Molar refractivity	1			0.271791	1.147561	3.32E-05
AATSC7c: Average centered Broto-Moreau autocorrelation - lag 7 / weighted by charges	-0.21199	1		-0.00886	1.051805	0.001166
E3u: 3rd component accessibility directional WHIM index / unweighted	0.288869	0.001659	1	0.737073	1.095995	3.95E-05

Prediction and validation of the activity of designed compounds

The designed compounds were drawn and optimized the same protocol as earlier described in chapter 2 of this work (Figure 4). The designed compounds after optimization using Spartan were converted to SDF file and the PadelDrecriptor software was used to calculate their respective descriptors. The descriptors used in developing the models presented in Table SD2 were selected for each designed compound and fitted into the built model (Eq. 7) and the activity of each designed compound was predicted, the predicted activity of each compound is shown in Table 3. The leverages of each of the compounds were also calculated using Eq. 6, presented in Table 3, it could be observed that the compounds C-145 and C-205 had leverage values greater than the threshold value of 0.63 obtained for the model using Equation 5 despite having predicted activity better than their respective templates with compounds C-145, C-148, C-151, C-152 C-153, C-1702, C-203, C-205, and C-206 having predicted activity (pI) values of 0.4098, 0.6345, 0.4116, 0.5112, 0.3307, 0.4193, 0.6036, 0.7597 and 0.6736 respectively presented in Table 3. Among the designed compounds, C-148, C-203, C-205, and C-206 have better activity (pI) than the selected lead compound (7n) [15] with the experimental activity of 0.602 (Table SD1), hence more potent than the lead.
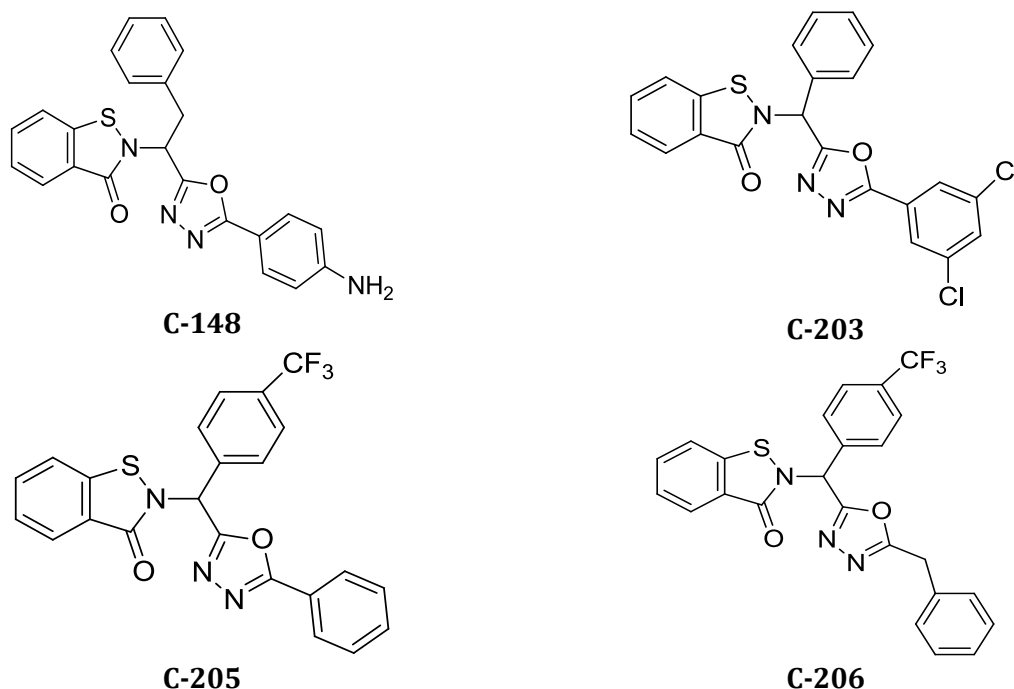
Figure 4. Structure of the most active designed compounds

Table 3. The designed compounds' descriptors, as well as their predicted biological activities and leverages

S/N	ID	AMR	AATSC7c	E3u	Predicted activity	Leverages (threshold h* = 0.63)
1*	C-145	130.9199	-6.82E-04	0.482132	0.409826	0.842483
2	C-148	129.2552	-0.00108	0.498872	0.634487	0.194995
3	C-151	127.1149	3.85E-04	0.4987	0.41163	0.261052
4	C-152	126.9272	1.56E-04	0.504766	0.511292	0.244369
5	C-153	126.9272	8.65E-04	0.497258	0.330782	0.409418
6	C-172	128.2008	6.16E-04	0.500076	0.41934	0.461948
7	C-203	130.2724	-8.49E-04	0.497173	0.603629	0.355408
8*	C-205	126.0545	-0.00135	0.511008	0.759729	0.826299
9	C-206	130.6037	-0.00138	0.497006	0.673676	0.404027

Docking Simulation Studies of the designed compounds

Understanding how the proposed compounds interact with the therapeutic target is crucial to understanding its observed inhibitory biological activity against the DENV protease (3UI1). All the designed BTZO derivatives were subjected to a molecular docking calculation, which is a useful computational approach for describing the interaction of drugs on a specific therapeutic target. The main data set (BTZO) which consists of 24 derivatives were additionally docked with the target to substantiate the evidence of our result.

Due to the absence of a specific FDA (US Food and Administration) approved drug for the treatment of DENV related infections, Ribavirin, which is a broad-spectrum anti-viral drug was also docked with the target as a standard inhibitor with the proven antiviral property. To also corroborate our findings with experimental data, a well-known plant source inhibitor called Panduratin A with a reported interaction as the

native ligand with the NS2B/NS3 receptor active site was also considered in the docking process as a standard [42].

The individual docking score (binding energy) interaction terms of the 24 BTZO derivative, as well as those of the designed derivative using the IC-M Pro, are presented in Tables SD5 and SD6 respectively. Figure 5 shows the DENV co-crystallized native ligand interacting with the amino acid residue and that of the docked most potent designed compound (148), it could be observed that the designed compounds have common interaction with that of the native ligand with the active site such as

The results of the docking using the IC-M Pro showing various interaction energy terms for the designed compounds are presented in Table 4. The 2D interaction with the active site amino acid of the receptor is shown in Figures 6a-6f. The designed compounds were observed to interact favorably with the various amino acids of the main active sites of the receptor through various interaction forms, such that compounds C-145, C-148, C-151, C-152, C-153, C-172, C-203, C-205 and C-206 as well as Panduratin and Ribavirin were found to form convention/carbon hydrogen bond with important amino acid residue of the active site of the protease (Gly153/Trp50)), (Gly153, Tyr161, Phe130, Lys131, Tyr150/Asn152), (Met84, Ser135, Gly153, Tyr161/Thr83, Asn152, Gly151), (Met84, Gly153, Tyr161/Thr83, Asn152, Gly151), (Ser135, Gly153, Tyr161, Tyr161/Asp129, Phe130, Gly151), (Met84, Gly153, Tyr161/Thr83, Asn152, Asn152), (Met84, Gly153, Tyr161/Thr83, His51, Asn152, Asn152), (Met84, Gly153/Thr83, Trp50, Asn152, Asn152), (Met84, Gly153, Thr83, Trp50/Asn152, Asn152), (Gly153, Gly153, Tyr161, Asn152, Gly153 /Met84, Met84) and (Gly133, Thr134, Gly153, Tyr161, Tyr161, Ser135, Asn152, RES1:H7, Phe130/Phe130) respectively while hydrophobic interactions were shown to occur involving important active site as well (Asp81, Asp81,

Val72, Asp75, His51, Tyr161) (His51), (His51, His51, Val155), (His51, Val155), (His51, Tyr150, Val155), (Tyr161, Val155), (Asn152, His51, Val155), (Asp81, Asp81, Val72, Asp75, Val155), (Asp81, Asp81, Asp75 Val155), (Tyr161, His51, His51, His51) and (His51, Tyr161) respectively (Table 4).

The results of the docking score of the designed compounds (C-148, C-203, C-205, and C-206) (Table 4) with better predicted biological than the best lead compound (7n) from the literature [15] are -23.731, -17.155, -20.210, -23.568 kcal/mol respectively, while other designed BTZO derivatives (C-145, C-151, C-152 C-153, and C-172) had a binding score of -12.5476, -21.1293, -20.3926, -16.3367 and -22.6789 kcal/mol respectively. Fortunately, most of the designed compounds had better binding scores than the standards (Panduratin and Ribavirin) with binding scores of -14.172 and -17.257 kcal/mol respectively. Based on the values of the binding score obtained for the designed compounds (Table 4) and those for the two standards (Panduratin and Ribavirin), it could be concluded that the designed compounds have better activity than the selected standard inhibitor of dengue virus and are hence more potent. Compound 148 is shown to be the most active owing to its better binding score than the parent BTZO derivative (Table SD5).

The docking investigation result revealed that all the designed compounds interacted favorably with the protease and could serve as inhibitors of the DENV, this could be seen from Figure 6a -6f in which 2D interactions for the proposed BTZO derivatives displayed favorable bond including the standards, as unfavorable bonds, influence the stability of ligand-protease complexes due to repulsive force within the complex. The designed BTZO derivatives were also found to interact with the common amino acid residues of the standard inhibitors as well as those of the co-crystallized native ligand of the protease (PDB code:3UI1). These residues have been reported

to form the important active pocket of the receptor as mentioned in the studies where DENV NS2B/N3 was considered as the therapeutic target, our designed compound interacts with the same amino residues in the catalytic active triad (His-51 Asp-75 and Ser-

135) proves it can inhibit the dengue virus, even outperforming selected standard inhibitors (Panduratin and Ribavirin). The outcome of our findings is in agreement with those obtained from previous studies on similar targets [42-44].

(a)   **(b)**
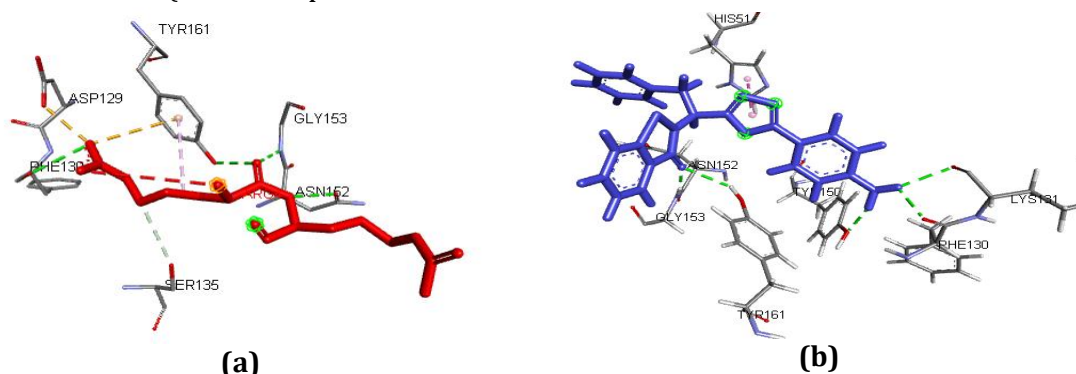
Figure 5. The native ligand (red) of the dengue virus receptor (PDB code: 3U1I) and the designed compound with the best anticipated biological activity (C-148) (blue) binding interaction

Table 4. The binding interactions of the designed compounds and the standard DENV NS2B/NS3 inhibitors (Panduratin and Ribavirin) with the target (PDB code: 3U1I)

Compound ID	Amino acid Residue	Interaction Distance (Å)	Type	(ΔG) Binding energy (kcal/mol)
C-145	GLY153	1.948	Conventional H Bond	-12.5476
	TRP50	2.736	Carbon H Bond	
	ASP81	2.858	Halogen (Fluorine)	
	ASP81	2.749	Halogen (Fluorine)	
	VAL72	3.458	Halogen (Fluorine)	
	ASP75	3.292	Halogen (Fluorine)	
	HIS51	3.768	Pi-Pi Stacked	
	TYR161	4.437	Pi-Pi Stacked	
C-148	GLY153	1.999	Conventional H Bond	-23.7313
	TYR161	2.615	Conventional H Bond	
	PHE130	2.216	Conventional H Bond	
	LYS131	2.511	Conventional H Bond	
	TYR150	2.057	Conventional H Bond	
	ASN152	2.882	Carbon H Bond	
	HIS51	3.774	Pi-Pi Stacked	
C-151	MET84	2.061	Conventional H Bond	-21.1293
	SER135	1.919	Conventional H Bond	
	GLY153	1.889	Conventional H Bond	
	TYR161	1.722	Conventional H Bond	
	THR83	2.825	Carbon H Bond	
	ASN152	2.617	Carbon H Bond	
	GLY151	2.847	Carbon H Bond	
	HIS51	2.929	Pi-Lone Pair	
	HIS51	4.877	Pi-Alkyl	
	VAL155	4.968	Pi-Alkyl	

Table 4. Continued

Compound ID	Amino acid Residue	Interaction Distance (Å)	Type	(ΔG) Binding energy (kcal/mol)
C-152	MET84	2.058	Conventional H Bond	-20.3926
	GLY153	1.884	Conventional H Bond	
	TYR161	1.689	Conventional H Bond	
	THR83	2.803	Carbon H Bond	
	ASN152	2.588	Carbon H Bond	
	GLY151	3.025	Carbon H Bond	
	D: HIS51	4.436	Pi-Alkyl	
	VAL155	4.975	Pi-Alkyl	
C-153	SER135	2.342	Conventional H Bond	-16.3367
	GLY153	1.823	Conventional H Bond	
	TYR161	2.614	Conventional H Bond	
	TYR161	2.706	Conventional H Bond	
	ASP129	2.645	Carbon H Bond	
	PHE130	2.406	Carbon H Bond	
	GLY151	2.726	Carbon H Bond	
	HIS51	2.321	Pi-Sigma	
	TYR150	5.445	Pi-Pi T-shaped	
	VAL155	5.302	Pi-Alkyl	
C-172	MET84	2.105	Conventional H Bond	-22.6789
	GLY153	1.974	Conventional H Bond	
	TYR161	1.605	Conventional H Bond	
	THR83	2.723	Carbon H Bond	
	ASN152	2.592	Carbon H Bond	
	ASN152	2.465	Carbon H Bond	
	TYR161	5.227	Pi-Alkyl	
	VAL155	5.011	Pi-Alkyl	
C-203	MET84	1.897	Conventional H Bond	-17.1554
	GLY153	1.862	Conventional H Bond	
	TYR161	1.673	Conventional H Bond	
	THR83	2.732	Carbon H Bond	
	HIS51	2.699	Carbon H Bond	
	ASN152	2.459	Carbon H Bond	
	ASN152	2.152	Carbon H Bond	
	ASN152	2.902	Pi-Sigma	
	HIS51	4.358	Pi-Alkyl	
	VAL155	5.350	Pi-Alkyl	
C-205	MET84	1.932	Conventional H Bond	-20.21
	GLY153	1.92637	Conventional H Bond	
	THR83	2.60668	Carbon H Bond	
	TRP50	2.76848	Carbon H Bond	
	ASN152	2.51497	Carbon H Bond	
	ASN152	2.16937	Carbon H Bond	
	ASP81	2.86867	Halogen (Fluorine)	
	ASP81	2.90848	Halogen (Fluorine)	
	VAL72	3.62076	Halogen (Fluorine)	
	ASP75	3.42414	Halogen (Fluorine)	
	VAL155	5.37552	Pi-Alkyl	

Table 4. Continued

Compound ID	Amino acid Residue	Interaction Distance (Å)	Type	(ΔG) Binding energy (kcal/mol)
C-206	MET84	1.93856	Conventional H Bond	-23.5677
	GLY153	1.92839	Conventional H Bond	
	THR83	2.60381	Carbon H Bond	
	TRP50	2.67662	Carbon H Bond	
	ASN152	2.53537	Carbon H Bond	
	ASN152	2.1725	Carbon H Bond	
	ASP81	2.95016	Halogen (Fluorine)	
	ASP81	3.06671	Halogen (Fluorine)	
	ASP75	3.50343	Halogen (Fluorine)	
	VAL155	5.33749	Pi-Alkyl	
Panduratin	GLY153	2.65662	Conventional H Bond	-14.1715
	GLY153	2.16462	Conventional H Bond	
	TYR161	1.62244	Conventional H Bond	
	ASN152	2.95797	Conventional H Bond	
	GLY153	1.9968	Conventional H Bond	
	MET84	2.82427	Carbon H Bond	
	MET84	2.96397	Carbon H Bond	
	TYR161	4.17375	Pi-Pi Stacked	
	HIS51	4.19149	Pi-Alkyl	
	HIS51	3.77429	Pi-Alkyl	
	HIS51	4.36968	Pi-Alkyl	
Ribavirin	GLY133	2.84341	Conventional H Bond	-17.2571
	THR134	2.11999	Conventional H Bond	
	GLY153	1.8523	Conventional H Bond	
	TYR161	2.49767	Conventional H Bond	
	TYR161	2.06805	Conventional H Bond	
	SER135	2.09271	Conventional H Bond	
	ASN152	2.25012	Conventional H Bond	
	RES1:H7	2.59186	Conventional H Bond	
	PHE130	2.32718	Conventional H Bond	
	PHE130	2.71699	Carbon H Bond	
	HIS51	3.29373	Pi-Donor H Bond	
	TYR161	2.99617	Pi-Lone Pair	
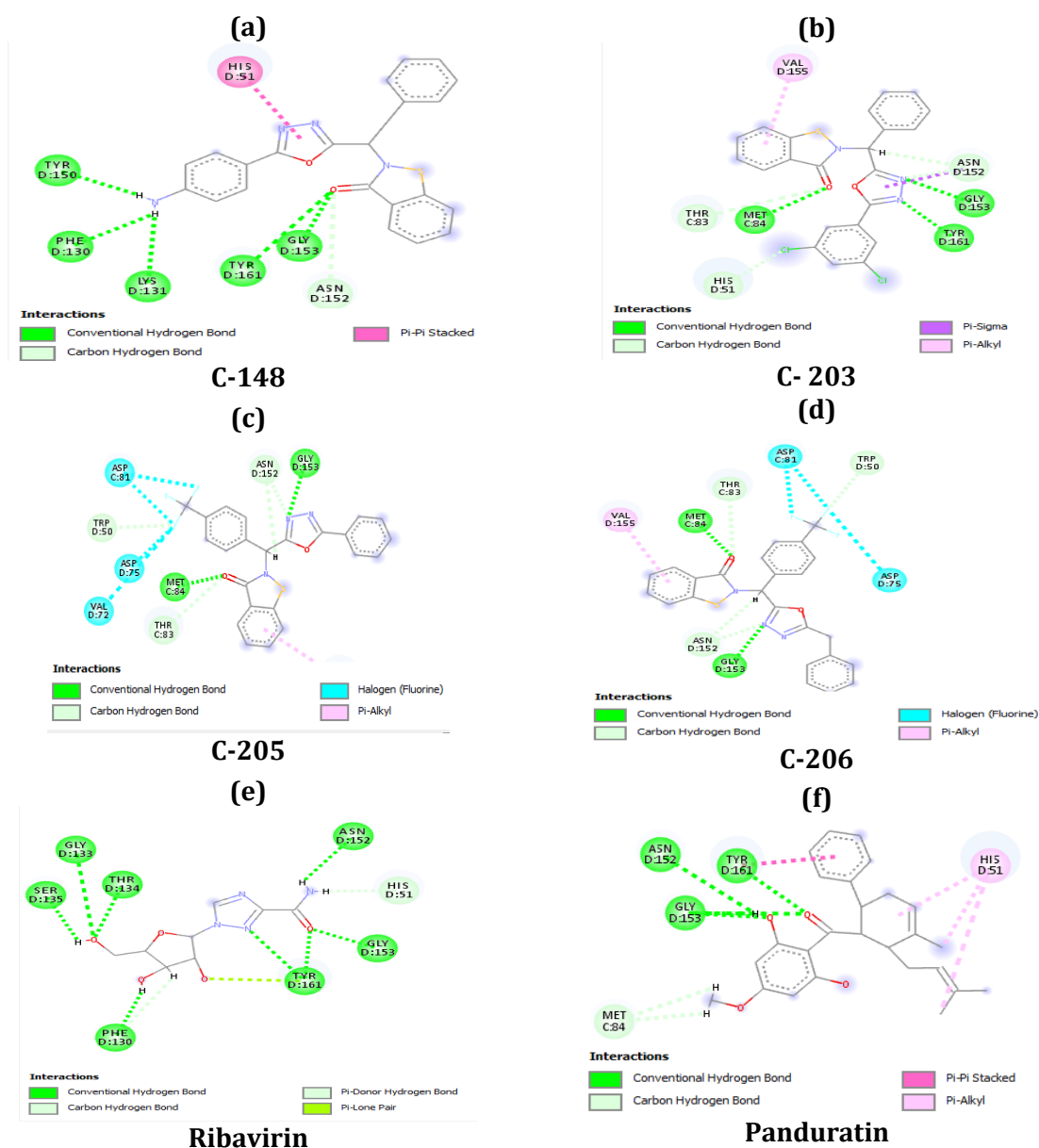
Figure 6. 2D binding interactions between the most active designed selected (C-148, C-203, C-205, C-206, Ribavirin, and Panduratin) compounds with the target protease (PDB entry: 3UI1)

Drug-likeness, pharmacokinetics, and ADMET profile of the designed BTZO derivatives

To avoid potential pitfalls related to pharmacokinetics and drug-likeness in the advanced development of any drug candidate, it is imperative to evaluate its pharmacokinetic profile. The pharmacokinetics evaluations and drug-likeness of the designed compounds using the *in-silico* approach through the Swiss-ADME web tool were investigated to explore their potentials as a proposed drug candidate. One of the well-known methods of bioavailability assessment of drug candidates proposed by Lipinski suggested that molecular weight not greater than 500, log p less than 5, hydrogen-bond donors of not more than 5, hydrogen-bond acceptors not more than 10, and topological polar surface area (TPSA) less than 140 was put into consideration.

The result of the predicted pharmacokinetic parameters is shown in Table 5, all the compounds were predicted to pass all the Lipinski's factors for oral bioavailability as indicated by their lower molecular weight, consensus log of less than five, the topological polar surface area of less than 140, as well as having hydrogen-bond donors and hydrogen-bond acceptors of less than five and ten respectively [45]. The non-violation of these rules by the designed compound entails acceptable bioavailability score and good drug-likeness of all designed compounds as shown by their scores presented in Table 5 [46].

The gastrointestinal absorption of all the designed compounds ranged between 94.51-97.77% (Table 5), whereas ribavirin had 48 % excellent and high intestinal tract absorption could be attributed to all the designed compounds better than even the standards. In the same way, the effect of important forms of P450 enzymes (CYP-1A2 CYP-3A4 and CYP-2D6) for drug metabolism was predicted [47], the results (Table 5) showed that all designed BTZO derivatives including the standard are non-inhibitors CYP-1A2 CYP-3A4 and CYP-2D6, except that compound C-203 that inhibits both CYP-1A2 CYP-3A4, as well as Panduratin which

inhibits CYP-2D6 cytochrome P450 enzymes. With exception of compounds C-151, C-203 C-205 including Ribavirin, the compounds are all Pgp substrates.

No PAIN alert was also observed in the investigation of all the compounds, negative PAIN alert (Table 5) indicates actual positive biological activity regardless of the protease [48].

The result of the toxicity studies is presented in Table 6, the toxicity evaluation of the designed compound revealed that all the compounds had no AMES toxicity except compounds C-151, C-152, and C-1702. Negative toxicity was obtained for compounds C-145, C-203, and the standard (Ribavirin). These compounds with negative AMES and hepatotoxicity could be considered non-carcinogenic (Table 6). Also, all the compounds including the standard inhibitors were all indicated to be non-inhibitor of hERG I. Oral Rat Acute Toxicity ranging between 2.28-2.45 mol/kg was obtained for all the compounds while the standard had an LD_{50} value of 1.48 mol/kg, making them less toxic than the standard inhibitor (Table 6). The valuable information indicated that the design can be proposed as potentially safe [49], and greener in general [50-52]. Interestingly, all the compounds are non-Renal OCTS substrates.

Table 5. Pharmacokinetics/ADME predictions of the designed compounds

ID	MLO GP	Pgp subs trate	CYP1A2 inhibitor	CYP2D6 inhibitor	CYP3A4 inhibitor	Lipinski #violations	Veber #violations	PAINS #alerts	Synthetic Accessibility
C-145	4.97	Yes	No	No	No	1	0	0	4.35
C-148	3.63	Yes	No	No	No	0	0	0	4.26
C-151	3.63	No	No	No	No	0	0	0	4.19
C-152	3.63	Yes	No	No	No	0	0	0	4.17
C-153	3.63	Yes	No	No	No	0	0	0	4.18
C-203	3.1	No	Yes	No	Yes	0	0	0	4.7
C-205	4.93	No	No	No	No	1	0	0	4.12
C-206	4.76	Yes	No	No	No	1	0	0	4.2
C-172	4.7	Yes	No	No	No	1	0	0	4.24
Panduratin	3.59	Yes	No	No	Yes	0	0	0	4.41
Ribavirin	-2.53	No	No	No	No	0	1	0	3.89

Table 6. Predicted toxicity, excretion, and intestinal absorption of the designed compounds

Compound ID	Some newly designed inhibitors of dengue virus N2B/NS3									Referenced inhibitors
	C-145	C-148	C-151	C-I52	C-153	C-203	C-205	C-206	C-172	Ribavirin
AMES toxicity	No	No	Yes	Yes	No	No	No	No	Yes	No
hERG I inhibitor	No	No	No	No	No	No	No	No	No	No
Carcinogenicity	No	No	Yes	Yes	No	No	No	Yes	No	No
Hepatotoxicity	No	Yes	Yes	Yes	Yes	No	Yes	Yes	Yes	No
Skin Sensitization	No	No	No	No	No	No	No	No	No	No
Oral Rat Acute Toxicity (LD50) (mol/kg)	2.47	2.68	2.56	2.53	2.78	2.33	2.49	2.55	2.46	1.48
Renal OCTS substrate	No	No	No	No	No	No	No	No	No	No
Intestinal adsorption (% Absorbed)	94.60	95.57	97.66	97.76	97.84	97.09	95.13	94.511	97.77	48.86

Conclusions

The application of computational tools in drug discovery has become of great interest to the pharmaceutical industry due to its low cost and efficiency. In this study, nine highly active and non-toxic inhibitors of the serine receptor of dengue virus responsible for the replication of the virus were designed through a ligand-based computational approach and validated through molecular docking as well as prediction of drug-likeness and ADMET parameter; a robust predictive QSAR was developed (R^2_{Train} = 0.89228, $R^2_{pred.}$ = 0.72734, R^2adj. = 0.87074, Q^2_{LOO} = 0.81896, and cR^2p = 0.8154). Compounds C-148, C-203, C-205, C-206 were predicted to have better biological activity (pI) of 0.634487, 0.603629, 0.759729, and 0.673676, which are all better than the lead compound (7n) with a value of 0.602 respectively, as well as molecular docking binding score of -23.731, -17.155, -20.210, -23.568 kcal/mol. A good docking interaction through conventional hydrogen bond and electrostatic interaction involving the most important active site amino acid residues of the DENV NS2B-NS3 protease (His-51, Asn-152, Tyr-161, Ser-135, Asp-75, Val-155, Gly-153, Met-84, and Thr-83) was observed to occur between the protease-ligand complexes similar to those of the standard inhibitors (Panduratin and Ribavirin), as well as those of the co-crystallized ligand of the DENV protease (PDB code:3UI1) and the compounds. The physicochemical, ADMET feature/pharmacokinetic analyses of the designed compounds revealed oral bioavailability, good ADME, and non-toxicity of the compounds with excellent intestinal adsorption. The 9 newly designed BTZO, demonstrated promising anti-DENV-2 activities and thus could be regarded as a potent DENV drug. This study was another giant stride towards assessing DENV NS2B-NS3 inhibition as possible targets for the development of innovative DENV infection therapeutics. This research findings point to BTZO's potential for further development as anti-dengue therapies. This breakthrough not only helped researchers better understand how BTZO hybrid compounds bind to these types of sites but also provide

information for the development of novel DENV NS2B-N3 protease inhibitors.

Acknowledgement

The authors gratefully acknowledged the technical effort of Mr. Moses of the Department of Chemistry, Ahmadu Bello University, Zaria.

Disclosure statement

No potential conflict of interest was reported by the authors.

ORCID

Samuel N. Adawara : 0000-0002-8789-7871
Gideon S. Adamu : 0000-0002-0700-9898

References

[1] S. Bhatt, P.W. Gething, O.J. Brady, J.P. Messina, A.W. Farlow, C.L. Moyes, J.M. Drake, J.S. Brownstein, A.G. Hoen, O. Sankoh, M.F. Myers, *Nature*, **2013**, *496*, 504–507. [CrossRef], [Google Scholar], [Publisher]

[2] S. Nie, Y. Yao, F. Wu, X. Wu, J. Zhao, Y. Hua, J. Wu, T. Huo, Y.L. Lin, A.R. Kneubehl, M.B. Vogt, *J. Med. Chem.*, **2021**, *64*, 2777–2800. [CrossRef], [Google Scholar], [Publisher]

[3] N.J. Barrows, R.K. Campos, K.C. Liao, K.R. Prasanth, R. Soto-Acosta, S.C. Yeh, G. Schott-Lerner, J. Pompon, O.M. Sessions, S.S. Bradrick, M.A. Garcia-Blanco, *Chem. Rev.*, **2018**, *118*, 4448–4482. [CrossRef], [Google Scholar], [Publisher]

[4] P. Simmonds, P. Becher, J. Bukh, E.A. Gould, G. Meyers, T. Monath, S. Muerhoff, A. Pletnev, R. Rico-Hesse, D.B. Smith, J.T. Stapleton, *J. Gen. Virol.*, **2017**, *98*, 2–3. [CrossRef], [Google Scholar], [Publisher]

[5] C. Nitsche, S. Holloway, T. Schirmeister, C.D. Klein, *Chem. Rev.*, **2014**, *114*, 11348–11381. [CrossRef], [Google Scholar], [Publisher]

[6] J.C. Saiz, M.A. Martín-Acebes, R. Bueno-Marí, O.D. Salomón, L.C. Villamil-Jiménez, J. Heukelbach, C.H. Alencar, P.K. Armstrong, T.M. Ortiga-Carvalho, R. Mendez-Otero, P.H. Rosado-de-Castro, *Front. Microbiol.*, **2017**, *8*, 1554. [CrossRef], [Google Scholar], [Publisher]

[7] H.J. Shin, M.H. Kim, J.Y. Lee, I. Hwang, G.Y Yoon, H.S. Kim, Y.C. Kwon, D.G. Ahn, K.D. Kim, B.T. Kim, S.J. Kim, *Microorganisms*, **2021**, *9*, 545. [CrossRef], [Google Scholar], [Publisher]

[8] J.P. Quek, S. Liu, Z. Zhang, Y. Li, E.Y. Ng, Y.R. Loh, A.W. Hung, D. Luo, C. Kang, *Antivir. Res.*, **2020**, *175*, 104707. [CrossRef], [Google Scholar], [Publisher]

[9] K. Sangeetha, M.A. Martín-Acebes, J.C. Saiz, KS Meena, *Microb. Pathog.*, **2020**, *149*, 104540. [CrossRef], [Google Scholar], [Publisher]

[10] S. Pach, T.M. Sarter, R. Yousef, D. Schaller, S. Bergemann, C. Arkona, J. Rademann, C. Nitsche, G. Wolber, *ACS Med. Chem. Lett.*, **2020**, *11*, 514–520. [CrossRef], [Google Scholar], [Publisher]

[11] S. Zhu, C. Zhang, L.S. Huang, X.Q. Zhang, Y. Xu, X. Fang, J. Zhou, M. Wu, R.T. Schooley, Z. Huang, J. An, *Molecules*, **2019**, *24*, 1465. [CrossRef], [Google Scholar], [Publisher]

[12] C.Q. Nguyen, T.H. Nguyen, T.T. Nguyen, T.B. Bui, T.T. Nguyen, N.T. Huynh, T.D. Le, T.M. Nguyen, D.T. Nguyen, M.T. Nguyen, M.Q. Pham, *J. Chem.*, **2021**. [CrossRef], [Google Scholar], [Publisher]

[13] J. Chen, H. Jiang, F. Li, B. Hu, Y. Wang, M. Wang, J. Wang, M. Cheng, *Comput. Boil. Chem.*, **2018**, *77*, 261–271. [CrossRef], [Google Scholar], [Publisher]

[14] S.N. Adawara, G.A. Shallangwa, P.A. Mamza, A. Ibrahim, *Sci. Afr.*, **2021**, *13*, e00907. [CrossRef], [Google Scholar], [Publisher]

[15] H. Lai, D. Dou, S. Aravapalli, T. Teramoto, G.H. Lushington, T.M. Mwania, K.R. Alliston, D.M. Eichhorn, R. Padmanabhan, W.C. Groutas, *Bioorg. Med. Chem.*, **2013**, *21*, 102–113. [CrossRef], [Google Scholar], [Publisher]

[16] Z. Li, H. Wan, Y. Shi, P. Ouyang, *J. Chem. Inf. Comput. Sci.*, **2004**, *44*, 1886–1890. [CrossRef], [Google Scholar], [Publisher]

[17] G. Pandey, A.K. Saxena, *J. Chem. Inf. Model.*, **2006**, *46*, 2579–2590. [CrossRef], [Google Scholar], [Publisher]

[18] B. Desai, D. Sureja, Y. Naliapara, A. Shah, A.K. Saxena, *Bioorg. Med. Chem.*, **2001**, *9*, 1993–1998. [CrossRef], [Google Scholar], [Publisher]

[19] W.J. Hehre, W.W. Huang, *Chemistry with computation: an introduction to SPARTAN*, Wavefunction, Incorporated, **1995**. [Google Scholar]

[20] C.W. Yap, *J. Comput. Chem.*, **2011**, *32*, 1466–1474. [CrossRef], [Google Scholar], [Publisher]

[21] P. Ambure, R.B. Aher, A. Gajewicz, T. Puzyn, K. Roy, *Chemometr. Intell. Lab. Syst.*, **2015**, *147*, 1–3. [CrossRef], [Google Scholar], [Publisher]

[22] R.W. Kennard, L.A. Stone, *Technometrics*, **1969**, *11*, 137–148. [CrossRef], [Google Scholar], [Publisher]

[23] D.E. Arthur, A. Uzairu, P. Mamza, E. Abechi, G. Shallangwa, *Albanian J. Pharm. Sci.*, **2016**, *3*, 4–9. [Google Scholar]

[24] A. Golbraikh, A. Tropsha, *J. Mol. Graph. Model.*, **2002**, *20*, 269–276. [CrossRef], [Google Scholar], [Publisher]

[25] K. Roy, R.N. Das, P. Ambure, R.B. Aher, *Chemometr. Intell. Lab. Syst.*, **2016**, *152*, 18–33. [CrossRef], [Google Scholar], [Publisher]

[26] T.I. Netzeva, A.P. Worth, T. Aldenberg, R. Benigni, M.T. Cronin, P. Gramatica, J.S. Jaworska, S. Kahn, G. Klopman, C.A. Marchant, G. Myatt, *Altern. Lab. Anim.*, **2005**, *33*, 155–173. [CrossRef], [Google Scholar], [Publisher]

[27] A. Afantitis, G. Melagraki, H. Sarimveis, P.A. Koutentis, J. Markopoulos, O. Igglessi-Markopoulou, *Bioorg. Med. Chem.*, **2006**, *14*, 6686–6694. [CrossRef], [Google Scholar], [Publisher]

[28] I. Mitra, A. Saha, K. Roy, *Mol. Simul.*, **2010**, *36*, 1067–1079. [CrossRef], [Google Scholar], [Publisher]

[29] Z.Y. Ibrahim, A. Uzairu, G. Shallangwa, S. Abechi, *SN Appl. Sci.*, **2020**, *2*, 1170. [CrossRef], [Google Scholar], [Publisher]

[30] C.G. Noble, C.C. Seh, A.T. Chao, P.Y. Shi, *J. Virol.*, **2012**, *86*, 438–446. [CrossRef], [Google Scholar], [Publisher]

[31] D.S. Biovia, Discovery studio modeling environment, release 2017, San Diego: DassaultSystèmes, **2016**. [Google Scholar]

[32] R. Abagyan, M. Totrov, D. Kuznetsov, *J. Comput. Chem.*, **1994**, *15*, 488–506. [CrossRef], [Google Scholar], [Publisher]

[33] S.N. Adawara, G.A. Shallangwa, P.A. Mamza, A. Ibrahim, *Chem. Afr.*, **2021**, *4*, 861–868. [CrossRef], [Google Scholar], [Publisher]

[34] D.E. Arthur, A.N. Samuel, S. Ejeh, S.E. Adeniji, O. Adedirin, M. Abdullahi, *Sci. Afr.*, **2020**, *10*, e00612. [CrossRef], [Google Scholar], [Publisher]

[35] A. Daina, O. Michielin, V. Zoete, *Sci. Rep.,* **2017**, *7*, 42717. [CrossRef], [Google Scholar], [Publisher]

[36] D.E. Pires, T.L. Blundell, D.B. Ascher, *J. Med. Chem.*, **2015**, *58*, 4066–4072. [CrossRef], [Google Scholar], [Publisher]

[37] S.N. Adawara, G.A. Shallangwa, P.A. Mamza, A. Ibrahim, *Beni-Suef Univ. J. Basic Appl. Sci.*, **2020**, *9*, 1–17. [CrossRef], [Google Scholar], [Publisher]

[38] A. Gajewicz, *Environ. Sci. Nano*, **2018**, *5*, 408–421. [CrossRef], [Google Scholar], [Publisher]

[39] R. Todeschini, V. Consonni, *Handbook of molecular descriptors,* John Wiley & Sons, **2008**. [Google Scholar]

[40] O. Adedirin, A. Uzairu, G.A. Shallangwa, S.E. Abechi, *J. Eng. Exact Sci.*, **2018**, *4*, 0065–0084. [CrossRef], [Google Scholar], [Publisher]

[41] S. Adeniji, S. Uba, A. Uzairu, *Phys. Chem. Res.*, **2018**, *6*, 479–492. [CrossRef], [Google Scholar], [Publisher]

[42] M. Hariono, S.B. Choi, R.F. Roslim, M.S. Nawi, M.L. Tan, E.E. Kamarulzaman, N. Mohamed, R. Yusof, S. Othman, N. Abd

Rahman, R. Othman, *Plos One*, **2019**, *14*, e0210869. [CrossRef], [Google Scholar], [Publisher]

[43] S.K. Yusufzai, H. Osman, M.S. Khan, B.M. Abd Razik, M.O. Ezzat, S. Mohamad, O. Sulaiman, J.A. Gansau, T. Parumasivam, *Chem. Cent. J.*, **2018**, *12*, 1–6. [CrossRef], [Google Scholar], [Publisher]

[44] F. Batool, M. Saeed, H.N. Saleem, L. Kirschner, J. Bodem, *Pathogens*, **2021**, *10*, 464. [CrossRef], [Google Scholar], [Publisher]

[45] C.A. Lipinski, F. Lombardo, B.W. Dominy, P.J. Feeney, *Adv. Drug Deliv. Rev.*, **1997**, *23*, 3–25. [CrossRef], [Google Scholar], [Publisher]

[46] K. Tsaioun, S.A. Kates, *ADMET for medicinal chemists: a practical guide*, John Wiley & Sons, **2011**. [Google Scholar]

[47] P.F. Hollenberg, Drug Metab. Rev., **2002**, *34*, 17–35. [CrossRef], [Google Scholar], [Publisher]

[48] J.B. Baell, G.A. Holloway, *J. Med. Chem.*, **2010**, *53*, 2719–2740. [CrossRef], [Google Scholar], [Publisher]

[49] S.B. Olasupo, A. Uzairu, G.A. Shallangwa, S. Uba, *Futur. J. Pharm. Sci.,* **2021**, *7*, 63. [CrossRef], [Google Scholar], [Publisher]

[50] R. Safarkar, G. Ebrahimzadeh Rajaei, S. Khalili-Arjagi, *Asian J. Nanosci. Mater.*, **2020**, *3*, 157–166. [CrossRef], [Google Scholar], [Publisher]

[51] E. Rezaei-Aghdam, A. Shamel, M. Khodadadi-Moghaddam, G. Ebrahimzadeh Rajaei, S Mohajeri, *Asian J. Nanosci. Mater.,* **2021**, 188–200. [CrossRef], [Google Scholar], [Publisher]

[52] R. Fekri, S.A. Mirbagheri, E. Fataei, G. Ebrahimzadeh-Rajaei, L. Taghavi, *Anthropogenic Pollution*, **2021**, *5*, 93–103. [CrossRef], [Google Scholar], [Publisher]